Dynamics of functional failures and recovery in complex road networks

Xianyuan Zhan and Satish V. Ukkusuri*
Lyles School of Civil Engineering, Purdue University, West Lafayette, Indiana 47907, USA

P. Suresh C. Rao
Lyles School of Civil Engineering and Agronomy Department, Purdue University, West Lafayette, Indiana 47907, USA
(Received 6 February 2017; revised manuscript received 10 August 2017; published 1 November 2017)

We propose a new framework for modeling the evolution of functional failures and recoveries in complex networks, with traffic congestion on road networks as the case study. Differently from conventional approaches, we transform the evolution of functional states into an equivalent dynamic structural process: dual-vertex splitting and coalescing embedded within the original network structure. The proposed model successfully explains traffic congestion and recovery patterns at the city scale based on high-resolution data from two megacities. Numerical analysis shows that certain network structural attributes can amplify or suppress cascading functional failures. Our approach represents a new general framework to model functional failures and recoveries in flow-based networks and allows understanding of the interplay between structure and function for flow-induced failure propagation and recovery.

DOI: 10.1103/PhysRevE.96.052301

I. INTRODUCTION

Flow-induced functional failures are common phenomena in many human-engineered and natural flow-based networks. The functional performance of such networks is reflected by how efficiently flow is propagated across the network, and their functional failures are mostly due to flow overload (e.g., traffic congestion in transportation network, power surge in electric grids, flooding in drainage network). Traffic congestion in urban road networks is a typical case of a functional failure process in flow-based networks. It can be perceived as a form of temporary partial functional failure resulting from a high traffic load. Under congestion, certain segments of roads are temporarily closed or operating at a reduced efficiency, causing partial or full functional losses in the network. Compared with structural disruptions, functional failures such as traffic congestions are more frequent and pose significant operational and monetary loss to urban communities.

It is always desired to design infrastructure networks that suppress the emergence and cascading of functional failures. However, even the first step towards this goal, modeling the functional failure process and the resulting network performance, has been shown to be a difficult and not-well-understood problem. The structural characteristics and functional features of flow-based networks interact in complex ways that jointly determine how and where functional failures emerge, how the functional failures propagate, and how recovery occurs [1–8].

Traditional approaches to functional failure analysis seek to obtain the network functional performance by solving for flow patterns in the network using optimization-based methods [9,10] or traffic simulation [11,12]. This detaches network functional performances from structural details, leading to an incomplete understanding of the underlying mechanisms of the failure-recovery processes. Incorporating the propagation characteristics of real-world flows and their overloading behaviors in structural analysis has long been recognized as a challenging research question [13–15]. This is because the flow patterns in the network are governed by both the flow propagation principles (e.g., traffic equilibrium in traffic networks [9,10], routing behavior in information networks [16–18], minimum energy dissipation principle in river networks [19,20]) and the network structure [21]. Overlaying flow propagation principles on the structure of networks is difficult; it has been shown to be analytically tractable only in special cases, such as trees [20], starlike and homogeneous structured networks [14], and ring-and-hub structures [2,22]. To model functional failures and recoveries in real-world networks, new analytical tools need to be developed to capture the nontrivial interactions of network structure and functions.

We propose a vertex split-recovery model for examining traffic congestion evolution process in urban road networks. Unlike traditional studies, which distribute traffic flow in the network and use road capacities to identify congestion [9,10], the proposed model transforms congestion as a dynamic structural process in the network. The model is built on a dual representation of road networks augmented with functional states. We show that the congestion and recovery in a road network under this representation is equivalent to the splitting and coalescing of dual vertices. To construct the model, we collect high-temporal-resolution network traffic state data from two megacities in China (Beijing and Shanghai). Based on the insights from empirical observations, we model the vertex split-recovery process as a composite of four stochastic processes: (i) *self-splitting*, vertex split due to network-wide loading of traffic; (ii) *self-contagion*, where congestion propagates along the same roads (same dual vertex); (iii) *neighbor contagion*, where congestion cascades to neighboring roads (neighboring dual vertex); and (iv) *recovery*, where congestion in road segments recovers (coalescing of split dual vertices). The proposed model can explain the congestion evolution phenomenon in real-world data and provides new insights into the interplay of structure and function in flow-based networks.

*sukkusur@purdue.edu

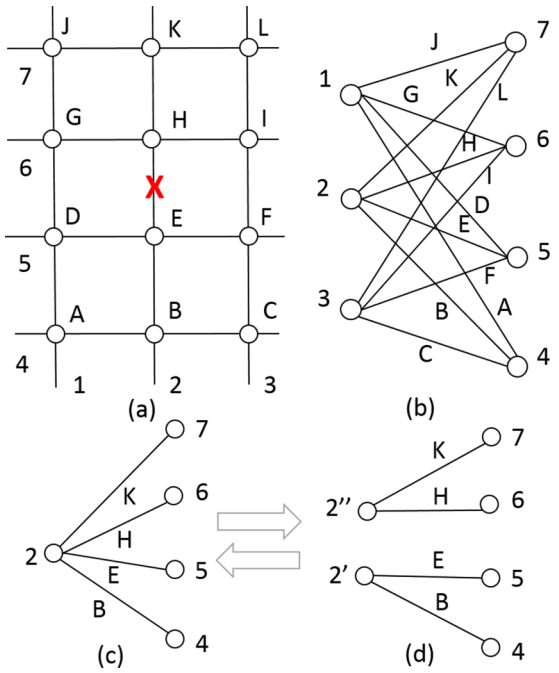

FIG. 1. Illustration of functional dual mapping and the vertex split-recovery process. (a) Primal representation of a road network; roads are labeled as numbers, and intersections as letters. (b) Dual representation of the road network in (a). (c), (d) Split and recovery of dual vertex 2 due to congestion on the HE segment of road 2.

II. FUNCTIONAL DUAL MAPPING AND VERTEX SPLIT-RECOVERY

Conventional representation of road networks perceives intersections as vertices and road segments as edges, referred to as primal networks. Recently, dual representation of road networks has gained more attention from researchers; it represents intersections as dual edges and merges individual road segments into meaningful stretches of roads represented as dual vertices based on certain criteria, e.g., axial direction, name of the street, road classes, and continuity [23–25]. The concept of dual representation is different from the "dual graph" in graph theory, which relates to the faces of planar graphs. The hierarchical intersection continuity negotiation (HICN) model [25,26] is among the best dual-representation approaches for road networks. According to HICN, two consecutive road segments belong to the same road if they have the same road class and the convex angle they form is close to 180°. The benefits of using dual representation are that dual-mapped networks are no longer constrained by planar embedding and uncover the underlying network hierarchy. For example, important roads in the network tend to be long and connected to many other roads, which leads to a large vertex degree in the dual-mapped network. An important finding is that both small-world and scale-free properties are observed in dual representation of road networks [23–25]. It is found that the dual-vertex degree distributions of different road networks have similar power-law exponents γ, varying between 2 and 3 [23,24].

We consider an extended form of HICN dual mapping that incorporates the functional states of the network, termed *functional dual mapping*. The key idea is to perform dual mapping on a function-state-encoded network. This treatment enables conversion of the congestion evolution, a functional process, into a structural process (see Fig. 1). Figure 1 provides an illustration of functional dual mapping. Consider road 2 in network G in Fig. 1(a); under dual representation, road 2 will be mapped to a dual vertex in Fig. 1(c) that consists of road segments KH, HE, and EB. Assume that road segment HE gets congested and temporarily loses its functional connectivity. From the functional perspective, the current network is equivalent to a network with road segment HE removed (referred to as G'). If dual mapping is performed on G', road 2 will be represented as two disconnected dual vertices, $2'$ and $2''$ in Fig. 1(d). Under functional dual mapping, the congestion and recovery on road segments are equivalent to dual-vertex splits and merging of the previously split dual

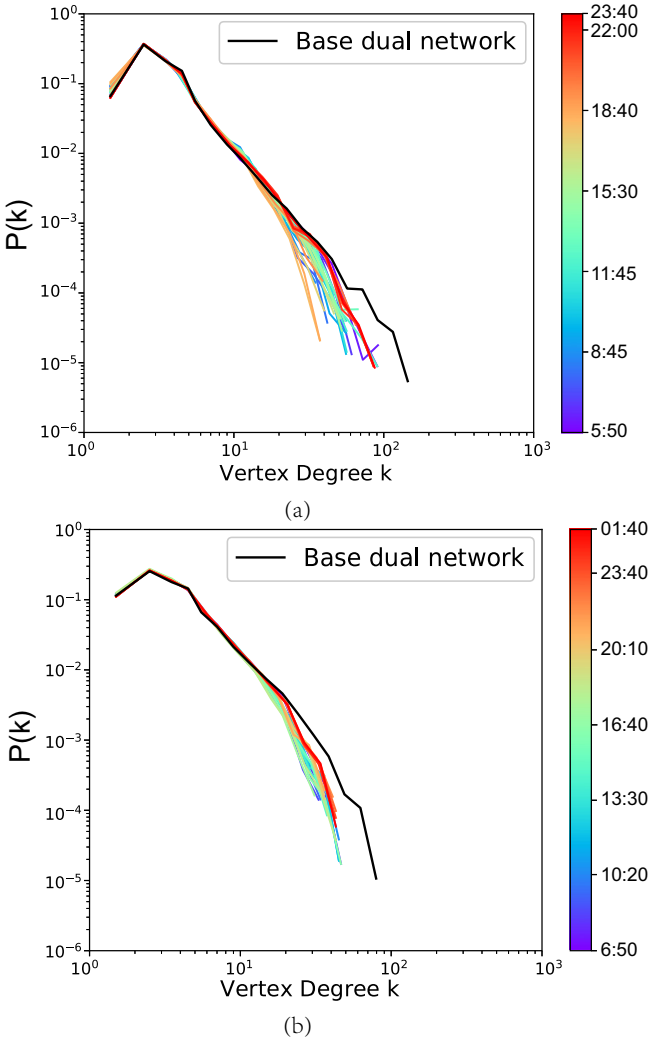

FIG. 2. Plots of the evolution of dual degree distributions for function-augmented dual networks: (a) Beijing road network (12/14/2015); (b) Shanghai road network (7/7/2016). The black line and the colored lines represent the degree distribution of the base dual network and the function-augmented dual networks at different times of day. Logarithmic binning is used for better clarity. The degree distribution of the base dual network can be fitted to a power-law distribution, $p(k) \sim k^{-\gamma}$, for $k \geqslant k_{\min} = 3$, $\gamma = 2.58$ (Beijing) and $k \geqslant k_{\min} = 4$, $\gamma = 2.48$ (Shanghai).

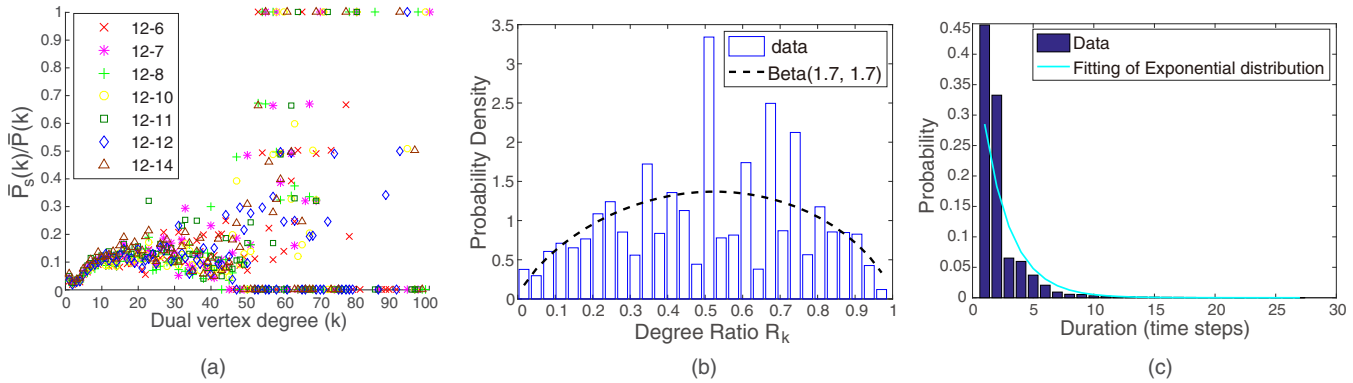

FIG. 3. Behavior of the vertex split-recovery process using the 7-day congestion evolution data from the Beijing road network. (a) Plot of the normalized vertex- split probability. The y axis is the normalized vertex-split probability $\bar{P}_s(k)/\bar{P}(k)$. $\bar{P}(k)$ and $\bar{P}_s(k)$ are the average proportions of degree k dual vertices and degree k dual vertices with vertex split in the function-augmented dual networks. Both $\bar{P}(k)$ and $\bar{P}_s(k)$ are obtained by averaging the results from function-augmented dual networks at all time steps during the day. (b) Probability distribution of the degree ratio R_k for binary vertex splits, which can be fitted to a beta distribution [$\beta(1.697,1.697)$]. (c) Distribution of the duration time t between the time at which the vertex gets split and the time at which it recovers, which can be approximated by an exponential distribution.

vertices in functional dual-mapped networks (referred to as *function-augmented dual networks*). We refer to the original dual-mapped network as the *base dual network* $G_D(V_D, E_D)$, which corresponds to the network without any congestion.

To track the dynamic vertex split-recovery process that represents the congestion evolution, functional dual mapping is applied and creates a series of function-augmented dual networks $G_D^t(V_D^t, E_D^t)$ for each time step t (see Appendix A). The variations of dual degree distributions within a day for the function-augmented dual networks is shown in Fig. 2. The degree distribution of the base dual network can be fitted to a power-law distribution, $p(k) \sim k^{-\gamma}$ for $k \geqslant k_{\min}$. In the function-augmented dual network, high-degree dual vertices are more likely to experience vertex split, causing faster probability decay at the tail. This leads to deviation of the power-law distribution but can be better fitted to a power law with an exponential cutoff distribution, $p(k) \sim k^{-\gamma} e^{-\kappa k}$.

III. EMPIRICAL OBSERVATIONS

To explore the behavior of the real-world vertex split-recovery process, we perform empirical analyses using network congestion evolution data from two megacities in China: Beijing (the road network within the fourth ring road contains 17 148 road segments) and Shanghai (the road network within the middle ring road contains 18 173 road segments). The network-wide link travel times of these two megacities were collected from an online digital map service in China (Baidu Map) every 40–60 min from 06:00 to 24:00 using a data crawler, which allows for tracking of the congestion evolution on an hourly basis (Beijing, around 40 min; Shanghai, around 60 min). Seven days of network state data from Beijing road network in December 2015 (12/6–12/8, 12/10–12/12, and 12/14) and six days of data from Shanghai in July 2016 (7/7, 7/9–7/13) were collected. All road travel time data were converted to road speeds. The collected link travel times were further compiled into binary functional states (failed state 0, congested; working state 1, not congested) at each time step. We identify a link as congested when its speed is less than 20% of its speed limit. For simplicity, we model the road network as an undirected network. For a road segment that carries bidirectional traffic, we consider the segment in the failed state if traffic in either of the two directions gets congested. Figure 3 presents some observed behaviors of the vertex split-recovery process using the 7-day congestion evolution data from the Beijing road network.

The vertex degree and splitting histories of dual vertices are found to be the two major factors governing the vertex-splitting process. Important roads in the network usually serve as backbones of the network and tend to have high vertex degrees in the dual-mapped network. These roads are more likely to carry a larger amount of traffic and, thus, prone to congestion. Figure 3(a) confirms the intuition that the overall normalized vertex-split probability shows a positive correlated trend with the dual-vertex degree, especially low-degree dual vertices. Extreme probability values (0 and 1) for high-dual-degree vertices are caused by their small sample sizes. There are only one or two such dual vertices in function-augmented dual networks at specific time steps, and they are thus more likely to yield a probability of 0 or 1.

Numerical analysis also reveals the facilitative impact of splitting history on future vertex splits. Suppose a dual vertex is split at some time step, and then congestion is more likely to propagate along the same road as well as to neighboring roads, causing further vertex splits at later time steps. Some typical examples of this phenomenon are the propagation of traffic kinematic waves [27] and the queue spillover on oversaturated roads [28]. It is observed that the conditional probability of vertex split under the existence of vertex split of the original dual vertex (self-split) in the previous time step [P(split|has previous split) = 0.23] is significantly higher than in the case where there are no previous self-splits [P(split|no previous split) = 0.03]. Similarly, the conditional vertex-split probability under the existence of neighbor splits in the previous time step [P(split|has previous neighbor split) = 0.05] is about twice as high as in the case where none of the neighboring dual vertices split [P(split|no previous neighbor split) = 0.03]. This

phenomenon is also related to the formation of gridlock in road networks [29], where traffic congestion spreads across neighboring roads and causes severe local network functional failure. Both observations confirm that a split history increases the vertex-split probability, and the impact of historical self-split is much larger than that of splits occurring in neighboring dual vertices.

We also examined the changes in dual degree after each vertex is split. To simplify the analysis, we considered only binary splits. If there are multiple vertex splits at a time step, we decompose them into a series of binary vertex splits. For each binary split, assume that the original dual vertex of degree k splits into two subvertices of dual degree k' and k'', the ratio $R_k = k'/k$ (referred to as the degree ratio) is found to be roughly approximated by a symmetric beta distribution, $\beta(\beta+1,\beta+1)$ [Fig. 3(b)], where $\beta \sim 0.7$. This indicates that the conditional split probability of a degree k dual vertex can be modeled as $P(k'|k) \propto [k'(k-k')]^{\beta}$. It suggests that dual vertices are more likely to split into two dual vertices with similar dual degrees rather than highly unbalanced dual degrees.

Figure 3(c) presents the distribution of the time duration for a split vertex to recover. The time duration is measured as the number of data collection steps (around 40 min for the Beijing road network). Due to Internet delay during the data collection process, the actual length of each time step can be slightly different (typically 2–5 min). It is found that the duration time t can be approximated by an exponential distribution $[P_c(t) = \theta e^{-\theta t}, t > 0]$. The recovery process can be captured using a remarkably simple statistical distribution which is common in modeling the survivor times of many physical, biological, and economic processes [30,31]. Moreover, the exponential duration-time distribution for dual vertices that remain in the split condition also implies a constant recovery rate in the system.

IV. VERTEX SPLIT-RECOVERY MODEL

We propose a vertex split-recovery model for the functional failure process in urban road networks based on the equivalent representation of road congestion and vertex split-recovery. We introduce the following model assumptions based on the insights from the previous empirical observations:

(1) *No splitting of degree 1 dual vertices*.

(2) *Binary split and no degree loss*: A dual vertex of degree k splits into two subvertices of degrees i and $k-i$.

(3) *Conditional splits*: The resulting degree of the split subvertices of a dual vertex of degree k follows some conditional splitting probability distribution $P(i,k-i|k)$.

(4) *Self-splitting*: Each dual vertex can split at some self-split rate $\rho(k,\eta(t))$ due to the network loading of flow, where $\eta(t)$ is a functional measure of the network loading level at time t. We further assume that $\rho(k,\eta(t)) = (k-1)\eta(t)$.

(5) *Self-contagion*: If a dual vertex of degree k has an unrecovered split, it will continue splitting at rate $g(k) = \tau(k-1)$, where τ is a fixed rate.

(6) *Neighbor contagion*: A split dual vertex will cause its neighbor to split at a fixed rate λ. Moreover, if the neighboring dual vertex of degree k already splits into subvertices, the impact on each subvertex of degree k_i is $\lambda\frac{k_i-1}{k-1}$ (ratio of the potential number of splits for the subvertex to that for the original dual vertex).

(7) *Recovery*: Each vertex split recovers at a fixed rate θ.

With the above model assumptions, we can simulate the vertex split-recovery process in the function-augmented dual network. However, directly solving the detailed network configuration at a particular time step will be analytically intractable. Instead, we are interested in the expected stationary solution of the vertex split-recovery process in the stable state under a constant network loading level $[\eta(t) = \eta]$. This solution is relatively easy to obtain while providing sufficient insights about the final impact of the vertex split-recovery process. In the following, we present a two-level model to obtain this expected stationary solution. The microscopic-level model characterizes the expected behavior for a degree k dual vertex after S splits and focuses only on an individual dual vertex. The macroscopic-level model characterizes the evolution of the number of splits for each dual vertex in the entire network.

A. Microscopic-level model

If we remove the recovery history of the dual vertex (if a dual vertex has split but later recovered, we ignore this split) until time t, the splitting history of a dual vertex can be represented as a *ranked planar Markov branching tree* [32]. Markov branching trees were introduced by Aldous [33] as a class of random binary or multifurcating phylogenetic models, which is widely used in phylogenetic studies [33–35]. A *ranked plane tree* is defined as a tree where we distinguish the left and right child vertices of an internal vertex, and every internal vertex is labeled by an integer keeping track of the ordering in which the splits occur during the construction of the tree. The internal ordering is necessary in our case, since each dual vertex is comprised of an ordered set of road segments, and such ordering is preserved during the vertex splits caused by functional failures. Figure 4 presents an illustration of the ranked planar tree representation of the vertex-splitting history.

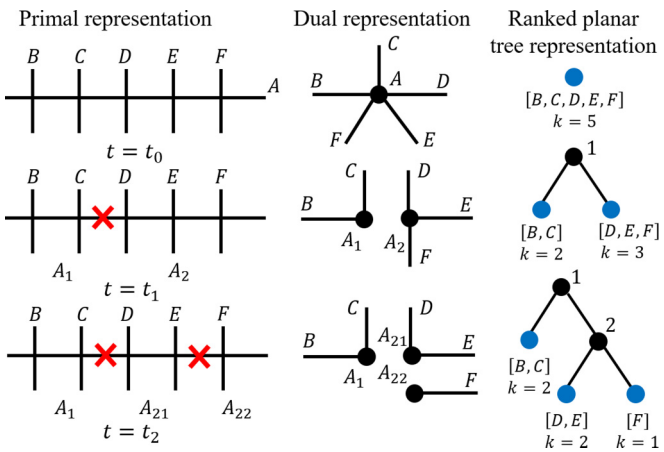

FIG. 4. Illustration of the ranked planar tree representation of the vertex-splitting history. Road A (dual degree $k = 5$) experiences congestion at time t_1 and t_2, which results in two dual-vertex splits. Under the ranked planar tree representation, it can be represented as two consecutive branchings of the tree.

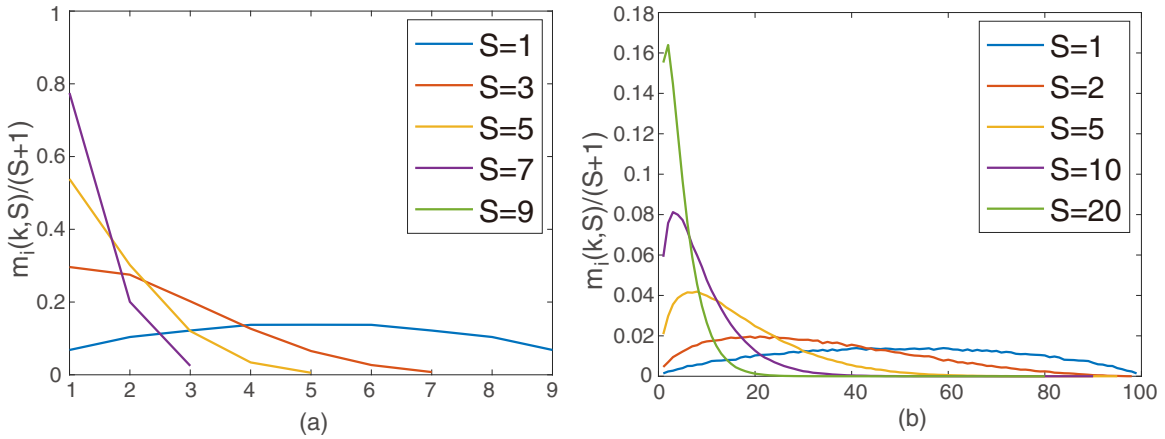

FIG. 5. Monte Carlo simulation results of the expected proportion of the degree i split subvertices after S splits $[m_i(k,S)/(S+1)]$ for degree k dual vertices: (a) $k = 10$; (b) $k = 100$. Computed using 50 000 simulation runs of the generating process of the microscopic-level model.

Here we consider a special generating process that approximates the ranked planar tree for the splitting history of a dual vertex of degree k having S splits:

(i) First split: The first split partitions the dual vertex into leaf vertices of degree k_1 and $k - k_1$ according to the conditional splitting distribution $P(k_1, k - k_1|k)$.

(ii) At the ith split: In all leaf vertices, selecting a leaf vertex j of degree k_j with a probability proportional to $k_j - 1$. Split vertex j into two new leaf vertices of degree k_{j1} and $k_j - k_{j1}$ according to $P(k_{j1}, k_j - k_{j1}|k_j)$.

(iii) Stop after all S splits are performed.

Based on the empirical observations, we define that the conditional splitting distribution has the form $P(i, k - i|k)$. That is,

$$P(i,k-i|k) = \frac{[i(k-i)]^\beta}{\sum_{j=1}^{k-1}[j(k-j)]^\beta}. \tag{1}$$

When $k \to \infty$, the normalized splitting location i/k asymptotically follows a symmetric beta distribution $[\beta(\beta+1, \beta+1)]$. This generative process is similar to the incremental construction method in the beta-splitting model for evolutionary trees proposed by Sainudiin and Véber [32], which constructs the evolutionary tree by incrementally partitioning an interval (vertices are represented as intervals). The value of β represents different splitting behaviors:

(i) $\beta = 0$, uniform split: The split location is chosen uniformly at $k - 1$ possible locations.

(ii) $\beta > 0$: The favored split location is in the middle section. This is the case reflected in the empirical observation, where we have $\beta \sim 0.7$.

(iii) $\beta < 0$: The favored split location is at the two ends.

In the microscopic-level model, we are interested in the expected degrees of leaf vertices for a degree k dual vertex after S splits. Define $M(k,S) = [m_1(k,S), m_2(k,S), \dots]^T$, where $m_i(k,S)$ is the expected number of split subvertices of degree i for a dual vertex of degree k after S splits. For $S = 1$, it can be easily shown that

$$m_i(k,1) = \begin{cases} \frac{2[i(k-i)]^\beta}{\sum_{j=1}^{k-1}[j(k-j)]^\beta}, & i < k; \\ 0, & i \geqslant k. \end{cases} \tag{2}$$

For $S > 1$ and $i = 1,2,\dots,k-S-1$, it can be proved that the following recursive formulation holds (see Appendix B):

$$m_i(k,S+1) = \frac{k-S-i}{k-S-1} m_i(k,S) + \frac{1}{k-S-1}\sum_{s=i+1}^{k-S}(s-1)m_s(k,S)m_i(s,1). \tag{3}$$

Although the closed-form expression for the above recursive formulation is only known for the reduced case $\beta = 0$ (see Appendix C), $m_i(k,S)$ can be computed by recursively solving Eq. (3) or using a Monte Carlo simulation based on the generating process. Numerical tests show that the expected degree distribution for the split subvertices $\frac{m_i(k,S)}{S+1}$ asymptotically follows a beta distribution $\beta(\tilde{\alpha}(k,S), \tilde{\beta}(S))$, where $\tilde{\alpha}(k,S)$ increases monotonically with an increase in both k and S, and $\tilde{\beta}(S)$ decreases with an increase in S (Fig. 5).

B. Macroscopic-level model

The macroscopic-level model focuses on the entire network rather than individual dual vertices. It characterizes the evolution of the number of splits for each dual vertex in the entire network at stable state ($t \to \infty$) under a constant network loading level ($\eta(t) = \eta$). We model the evolution of the number of splits of a dual vertex v of degree k in the network as a continuous-time Markov chain involving k states $(0,1,\dots,k-1)$. Each state represents the number of splits S_v. To simplify the model, we further assume that the states can only increase or decrease S_v by 1 at each transition. This can be perceived as a special generalization of the susceptible-infected-susceptible model in epidemiology [36]. The differences are that the susceptible-infected-susceptible model considers only two states, susceptible and infected, and the transition between these two states, while in the macroscopic-level model, we have transitions among k states.

For a dual vertex v in the base dual network, let k_i be the degree of its ith child vertex after splitting. Define the sign function $\mathrm{sgn}(S_v) = 1$ if $S_v > 0$ and 0 otherwise. The rate of transition between states can be modeled as follows:

(i) Transition rate from $S_v \to S_v + 1$ $(S_v < k-1)$:

$$\sum_{i=1}^{S_v+1}\left[\rho(k_i,\eta) + g(k_i)\mathrm{sgn}(S_v) + \lambda\frac{k_i-1}{k-1}\sum_{(u,v)\in E_D}\mathrm{sgn}(S_u)\right] = (k-1-S_v)\left[\eta + \tau\cdot\mathrm{sgn}(S_v) + \frac{\lambda}{k-1}\sum_{(u,v)\in E_D}\mathrm{sgn}(S_u)\right]. \quad (4)$$

(ii) Transition rate from $S_v \to S_v - 1$ $(S_v > 0)$: θS_v.

Equation (4) computes the overall rate of increase in S_v contributed by its $S_v + 1$ child vertices, where $\rho(k_i,\eta)$ and $g(k_i)\mathrm{sgn}(S_v)$ are the self-splitting and self-contagion rates of the ith child vertex, and $\lambda\frac{k_i-1}{k-1}\sum_{(u,v)\in E_D}\mathrm{sgn}(S_u)$ is the overall neighbor-contagion rate at the ith child vertex from all the split neighboring dual vertices $[\mathrm{sgn}(S_u) > 1]$.

Let probability distribution $X^v(t) = (x_0^v(t), x_1^v(t), \ldots, x_{k-1}^v(t))$, where $x_S^v(t)$ is the probability of dual vertex v at time t having S splits. Suppose all dual vertices initially do not have vertex splits $[x_0^v(0) = 1, \forall v \in V_D]$, using the previous transition scheme, the state equation for each dual vertex v at time t in the network can be written as

$$\begin{aligned}
\frac{dx_0^v(t)}{dt} &= -x_0^v(t)(k-1)\left[\eta + \frac{\lambda}{k-1}\sum_{(u,v)\in E_D}\mathrm{sgn}(S_u)\right] + \theta x_1^v(t),\\
\frac{dx_1^v(t)}{dt} &= -x_1^v(t)(k-2)\left[\eta + \tau + \frac{\lambda}{k-1}\sum_{(u,v)\in E_D}\mathrm{sgn}(S_u)\right] - \theta x_1^v(t) + x_0^v(t)(k-1)\left[\eta + \frac{\lambda}{k-1}\sum_{(u,v)\in E_D}\mathrm{sgn}(S_u)\right] + 2\theta x_2^v(t),\\
\frac{dx_S^v(t)}{dt} &= -x_S^v(t)(k-1-S)\left[\eta + \tau + \frac{\lambda}{k-1}\sum_{(u,v)\in E_D}\mathrm{sgn}(S_u)\right]\\
&\quad - S\theta x_S^v(t) + x_{S-1}^v(t)(k-S)\left[\eta + \tau + \frac{\lambda}{k-1}\sum_{(u,v)\in E_D}\mathrm{sgn}(S_u)\right] + (S+1)\theta x_{S+1}^v(t), \quad 1 < S < k-1,\\
\frac{dx_{k-1}^v(t)}{dt} &= x_{k-2}^v(t)\left[\eta + \tau + \frac{\lambda}{k-1}\sum_{(u,v)\in E_D}\mathrm{sgn}(S_u)\right] - (k-1)\theta x_{k-1}^v(t). \quad (5)
\end{aligned}$$

The state equations model the changes in $x_S^v(t)$ caused by four types of state transitions: (i) a decrease due to transition from S to $S+1$; (ii) a decease due to recovery from S to $S-1$; (iii) an increase due to transition from $S-1$ to S; and (iv) an increase due to recovery from $S+1$ to S.

Directly solving such a large coupled differential equation system is highly complex. We utilize the *degree-based mean-field* (DBMF) approximation [37–40] to gain some insights into the behavior of the stationary solution. The DBMF approximation for dynamical processes in networks assumes that all vertices of degree k are statistically equivalent. Under the DBMF approximation, we only need to consider $X^k(t) = (x_0^k(t), x_1^k(t), \ldots, x_{k-1}^k(t))$, where $x_S^k(t)$ is the proportion of degree k dual vertices that has S splits. Specifically, we consider two cases: (i) no degree correlation—the average probability that a dual vertex has a split neighbor at time t, $\phi(t)$, is the same for all dual vertices; and (ii) general degree correlation—the average probability that a dual vertex of degree k has a split neighbor, $\tilde{\phi}(t|k)$, depends on its degree.

1. DBMF approximation with no degree correlation

If we assume that there is no degree correlation in the network, then the overall neighbor-contagion rate for a dual vertex v of degree k can be approximated as [40,41]

$$\lambda\sum_{(u,v)\in E_D}\mathrm{sgn}(S_u) \simeq \lambda k\phi(t), \quad (6)$$

where $\phi(t)$ is the average probability that a dual vertex has a split neighbor at time t. If there is no degree correlation, $\phi(t)$ is given as [40]

$$\phi(t) = \sum_{k'>1}\frac{k'P(k')}{\langle k\rangle}(1 - x_0^{k'}(t)), \quad (7)$$

where $P(k)$ is the proportion of degree k dual vertices in the base dual network, and $\langle k\rangle$ is the average degree of the base dual network. The above expression gives the average probability of finding a split dual vertex following a randomly chosen dual edge. For simplicity, let

$$\Lambda_1^k(t) = \frac{\eta + \frac{\lambda k}{k-1}\phi(t)}{\theta}, \quad \Lambda_2^k(t) = \Lambda_1^k(t) + \frac{\tau}{\theta}. \quad (8)$$

Under the DBMF approximation, the state equations, Eq. (5), can be simplified as

$$\begin{aligned}
\frac{dx_0^k(t)}{dt} &= -x_0^k(t)(k-1)\theta\Lambda_1^k(t) + \theta x_1^k(t),\\
\frac{dx_1^k(t)}{dt} &= -x_1^k(t)(k-2)\theta\Lambda_2^k(t) - \theta x_1^k(t)\\
&\quad + x_0^k(t)(k-1)\theta\Lambda_1^k(t) + 2\theta x_2^k(t),\\
\frac{dx_S^k(t)}{dt} &= -x_S^k(t)(k-1-S)\theta\Lambda_2^k(t) - S\theta x_S^k(t)\\
&\quad + x_{S-1}^k(t)(k-S)\theta\Lambda_2^k(t) + (S+1)\theta x_{S+1}^k(t),\\
&\quad 1 < S < k-1,\\
\frac{dx_{k-1}^k(t)}{dt} &= x_{k-2}^k(t)\theta\Lambda_2^k(t) - (k-1)\theta x_{k-1}^k(t). \qquad (9)
\end{aligned}$$

We are interested in the stable proportion of dual vertices of degree k that has i splits $[x_i^k(t)]$ when $t \to \infty$, which corresponds to the stationary distribution of the continuous-time Markov chain. The stationary distribution can be analytically solved by setting $\frac{dx_S^k}{dt} = 0, \forall S = \{0,1,2,\ldots,k-1\}, \forall k$. Solving the system of equations, we obtain for $k > 1$

$$x_i^{k*} = \binom{k-1}{i}\Lambda_1^k\left(\Lambda_2^k\right)^{i-1}x_0^{k*}, \quad i = 1,2,\ldots,k-1, \qquad (10)$$

where Λ_1^k, Λ_2^k are $\Lambda_1^k(t)$, $\Lambda_2^k(t)$, with the $\phi(t)$ value taken at the stationary solution (ϕ^*). As $\sum_{i=0}^{k-1} x_i^{k*} = 1$, thus

$$\begin{aligned}
x_0^{k*} &= \left[1 + \frac{\Lambda_1^k}{\Lambda_2^k}\sum_{i=1}^{k-1}\binom{k-1}{i}\left(\Lambda_2^k\right)^i\right]^{-1}\\
&= \left[1 + \frac{\Lambda_1^k}{\Lambda_2^k}\left[\left(1+\Lambda_2^k\right)^{k-1} - 1\right]\right]^{-1}. \qquad (11)
\end{aligned}$$

Solving for ϕ^* using Eq. (7), we have

$$\begin{aligned}
\phi^* &= \frac{1}{\langle k\rangle}\sum_{k'>1}k'P(k')\\
&\quad\cdot\frac{-1+\left[1+\frac{\eta+\tau+\frac{\lambda k'}{k'-1}\phi^*}{\theta}\right]^{k'-1}}{\frac{\tau}{\eta+\frac{\lambda k'}{k'-1}\phi^*}+\left[1+\frac{\eta+\tau+\frac{\lambda k'}{k'-1}\phi^*}{\theta}\right]^{k'-1}}. \qquad (12)
\end{aligned}$$

The above nonlinear equation can be solved numerically. Using the solution of ϕ^*, we can obtain x_0^{k*} and x_i^{k*}.

2. DBMF approximation with the general degree correlation

When considering the general degree correlation, the overall neighbor-contagion rate can be approximated as

$$\lambda\sum_{(u,v)\in E_D}\mathrm{sgn}(S_u) \simeq \lambda k\tilde{\phi}(t|k), \qquad (13)$$

where $\tilde{\phi}(t|k)$ is the average probability that a degree k dual vertex has a split neighbor. It can be computed using $P(k'|k)$, the conditional probability of a degree k dual vertex that has a degree k' neighbor, as follows [40]:

$$\tilde{\phi}(t|k) = \sum_{k'}P(k|k')\left(1-x_0^{k'}\right). \qquad (14)$$

$P(k'|k)$ can be evaluated empirically from the actual base dual network, which incorporates more structural details of the network. Under this condition, the $\Lambda_1^k(t)$ and $\Lambda_2^k(t)$ in the no-degree-correlation case now become

$$\tilde{\Lambda}_1^k(t) = \frac{\eta + \frac{\lambda k}{k-1}\tilde{\phi}(t|k)}{\theta}, \quad \tilde{\Lambda}_2^k(t) = \tilde{\Lambda}_1^k(t) + \frac{\tau}{\theta}. \qquad (15)$$

It can be shown that the state equation, Eq. (9), still holds, but with $\Lambda_1^k(t)$ and $\Lambda_2^k(t)$ replaced by $\tilde{\Lambda}_1^k(t)$ and $\tilde{\Lambda}_2^k(t)$. The final stationary solutions can be derived as

$$x_i^{k*} = \binom{k-1}{i}\tilde{\Lambda}_1^k\left(\tilde{\Lambda}_2^k\right)^{i-1}x_0^{k*}, \quad i = 1,\ldots,k-1, \qquad (16)$$

$$x_0^{k*} = \left[1 + \frac{\tilde{\Lambda}_1^k}{\tilde{\Lambda}_2^k}\left[\left(1+\tilde{\Lambda}_2^k\right)^{k-1} - 1\right]\right]^{-1}, \qquad (17)$$

where $\tilde{\Lambda}_1^k$, $\tilde{\Lambda}_2^k$ are $\tilde{\Lambda}_1^k(t)$, $\tilde{\Lambda}_2^k(t)$, with $\tilde{\phi}(t|k)$ taking the value of $\tilde{\phi}(\infty|k)$ [$\tilde{\phi}(t|k)$ value at stationary solution x_i^{k*}].

Under the general degree correlation, there is no simple-form stationary solution due to the coupling of dual vertices of different degrees. The state equations for x_0^{2*}, x_0^{3*}, and $x_0^{k_{\max}*}$ now all become coupled, as the computation of $\tilde{\Lambda}_1^k$ and $\tilde{\Lambda}_2^k$ involves $\tilde{\phi}(\infty|k)$ and all $x_0^{k*}, k = 1,2,\ldots,k_{\max}$. However, x_i^{k*} is still numerically solvable for finite networks; it can be obtained by solving a large system of nonlinear equations involving Eqs. (14)–(17) for all dual-vertex degrees.

C. Dual-vertex degree distribution under the stationary solution

Combining the analytical results from the microscopic- and macroscopic-level models, the expected total numbers of dual vertices, N^*, and dual vertices of degree k, N_k^*, in the stable function-augmented dual network are

$$N^* = n\sum_{k=1}^{k_{\max}}P(k)\sum_{S=0}^{k-1}(S+1)x_S^{k*}, \qquad (18)$$

$$N_k^* = n\sum_{k'=k}^{k_{\max}}P(k')\sum_{S=0}^{k'-1}m_k(k',S)x_S^{k'*}, \qquad (19)$$

where n and $k_{\max}$ are the total number of dual vertices and the maximum degree in the base dual network. The expected degree distribution for the function-augmented dual network under stable conditions can thus be obtained as $P^*(k) = N_k^*/N^*$.

V. NUMERICAL RESULTS

A. Fitting to real-world data

The stationary solution of the vertex split-recovery model under the DBMF approximation is completely determined by three key parameters, namely, (i) the normalized network loading level $w_1(t) = \eta(t)/\theta$, (ii) the normalized self-contagion rate $w_2 = \tau/\theta$, and (iii) the normalized neighbor-contagion rate $w_3 = \lambda/\theta$. Here, $w_1(t)$ is a dynamic variable that measures the relative loading level of the entire network; w_2 and w_3 are fixed parameters governed by the network structure.

We fit the proposed model to empirical data to uncover the actual $w_1(t)$, w_2, and w_3 values in the test networks.

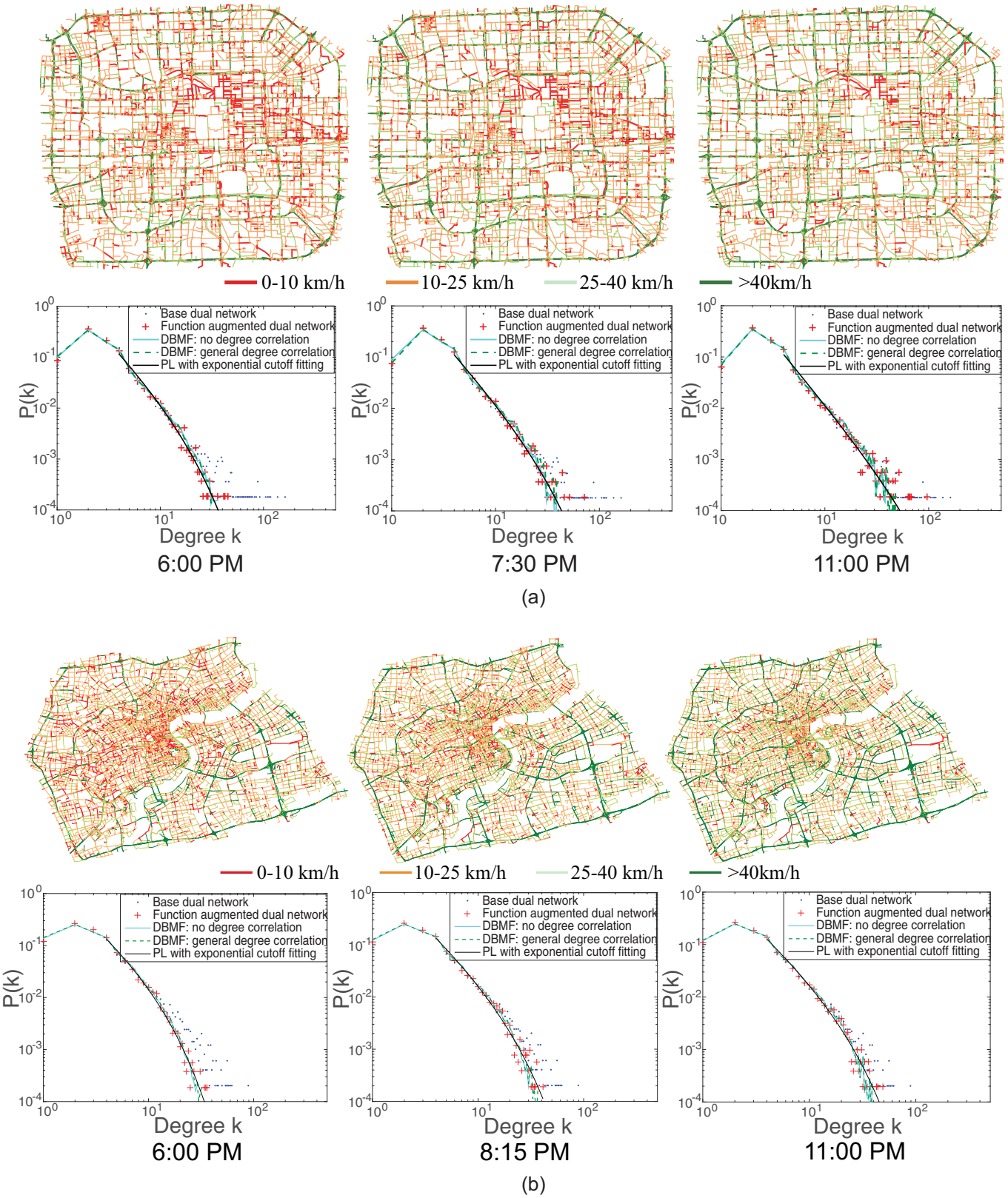

FIG. 6. Evolution of dual degree distributions for (a) the Beijing road network (12/10/2015) and (b) the Shanghai road network (7/11/2016). The top figures are the road speed plots at three sample time steps. The bottom figures present the corresponding dual-vertex degree distributions for (i) the base dual network (no congestion), (ii) the function-augmented dual network (actual congestion scenario), (iii) network configurations predicted by the vertex split-recovery model under different DBMF approximation schemes (no degree correlation and general degree correlation), and (iv) the power law with exponential cutoff fittings of the dual degree distributions.

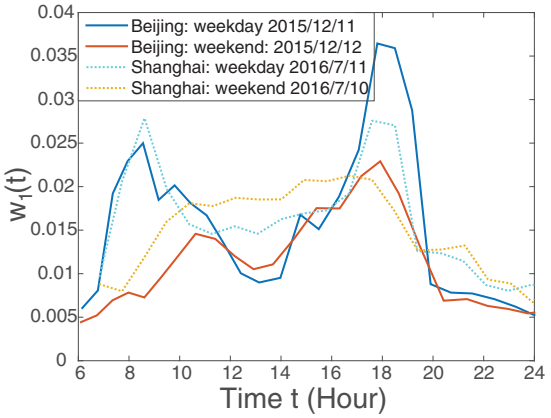

FIG. 7. Fitting result for $w_1(t)$ using the DBMF approximation with the general degree correlation.

The fitting is achieved by minimizing the overall statistical divergence between the model predicted and empirical dual degree distributions of the function-augmented dual networks. Let $P_T^*(k)$ and $Q_T(k)$ be the model predicted and empirical dual degree distribution for time period T. We minimize the overall statistical divergence of the two distributions over the entire day, defined as $\min_{w_1(t),w_2,w_3} \sum_T J(P_T^*||Q_T)$, where $J(P_T^*||Q_T)$ is the Jensen-Shannon divergence [42] between distribution P_T^* and distribution Q_T. Jensen-Shannon divergence is a popular measure for evaluating the dissimilarity between two probability distributions and widely used in statistics and information theory.

Figure 6 presents sample fitting results of the vertex split-recovery model (see the Supplemental Material for complete fitting results [43]). The larger extent of deviation for the dual-vertex degree distribution under severe congestion vs the no-congestion condition is clearly shown. It is illustrated that the vertex split-recovery model captures the expected behavior of the dual degree distribution of the function-augmented dual networks for both cities under different congestion levels. The fitted results for w_2 and w_3 are found to be different in the Beijing and Shanghai road networks, but within the same range. The mean and standard deviation of w_2 and w_3 in the Beijing road network under DBMF with no degree correlation are $\bar{w}_2 = 0.0744$, $\sigma(w_2) = 8.3 \times 10^{-3}$, $\bar{w}_3 = 4.3 \times 10^{-4}$, $\sigma(w_3) = 3.3 \times 10^{-4}$ [$\bar{w}_2 = 0.0687$,

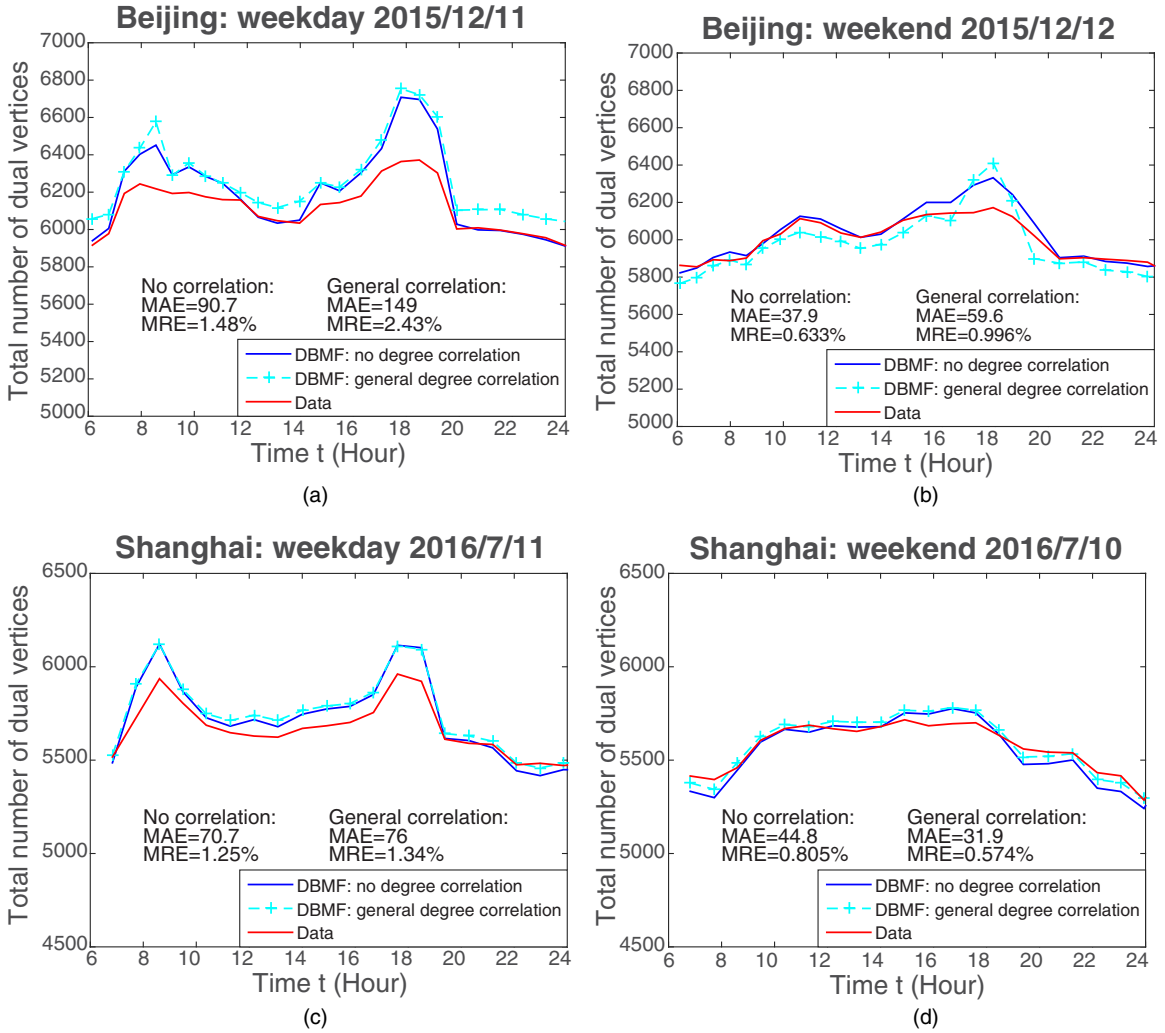

FIG. 8. Comparison of the total number of dual vertices from empirical data (red line) and the expected total number of dual vertices (N^*) obtained from the vertex split-recovery model for the Beijing and Shanghai road networks.

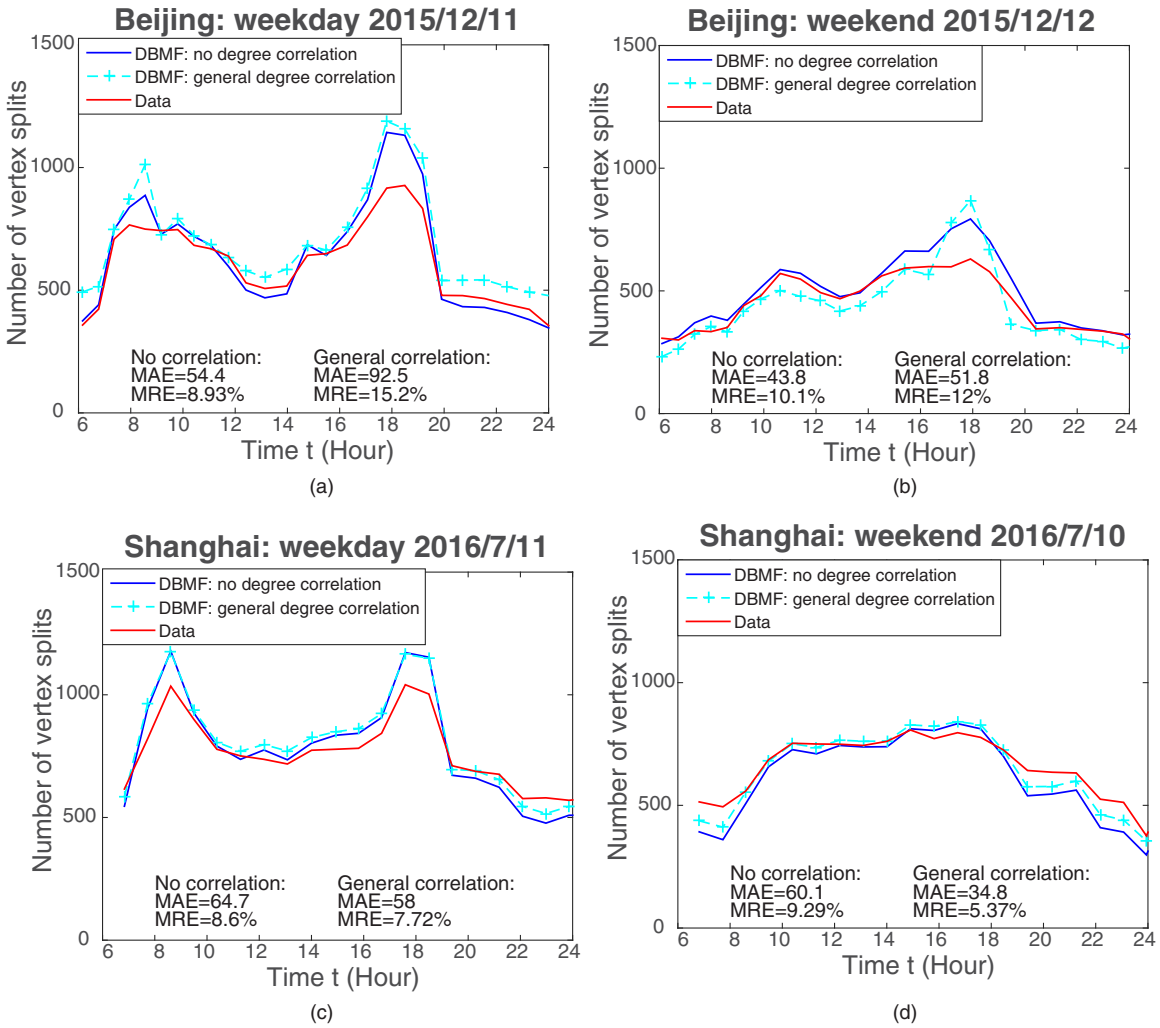

FIG. 9. Comparison of the total number of unrecovered vertex splits at each time step in the empirical data (red line) and the expected number of vertex splits (N^{ES}) obtained from the vertex split-recovery model for the Beijing and Shanghai road networks.

$\sigma(w_2) = 0.0109$, $\bar{w}_3 = 3.6 \times 10^{-4}$, $\sigma(w_3) = 2.0 \times 10^{-4}$ for DBMF with the general degree correlation]. The values for the Shanghai road network are $\bar{w}_2 = 0.125$, $\sigma(w_2) = 0.015$, $\bar{w}_3 = 5.0 \times 10^{-4}$, $\sigma(w_3) = 7.0 \times 10^{-6}$ [$\bar{w}_2 = 0.0915$, $\sigma(w_2) = 0.0099$, $\bar{w}_3 = 8.6 \times 10^{-4}$, $\sigma(w_3) = 4.0 \times 10^{-5}$ for DBMF with the general degree correlation]. The Shanghai road network exhibits larger w_2 and w_3 values than the Beijing road network does, likely because it has a more decentralized and homogeneous network structure. The Beijing road network has a typical ring-and-radial structure, where the major ring roads and radial expressways have a high traffic capacity, whereas the Shanghai road network is more gridlike. This makes congestion overall easier to propagate along the same or neighboring roads in the Shanghai road network (higher w_2 and w_3 values).

Figure 7 presents the evolution of fitted $w_1(t)$ for a typical weekday and a weekend for both the Beijing and the Shanghai road networks. It agrees well with the real-world network traffic loading level, where high traffic loading in the morning and evening peaks as well as low traffic loading in off-peak hours is well captured. Beijing and Shanghai showed slightly different traffic loading patterns, with higher traffic loading observed from noon to the early afternoon period (12:00–17:00) in the Shanghai network. These results show that $w_1(t)$ can be a good measure of the actual traffic loading level at network scale, which reflects the explanatory power of the vertex split-recovery model.

To further validate the vertex split-recovery model, we compare the total number of dual vertices and the vertex splits between the empirical data and the expected values obtained from the vertex split-recovery model. The expected number of vertex splits N^* is computed using Eq. (19), and the expected total number of vertex splits N^{ES} is computed as

$$N^{\mathrm{ES}} = n \sum_{k=2}^{k_{\max}} P(k) \sum_{s=1}^{k-1} s \cdot x_s^{k*}, \tag{20}$$

where x_s^{k*} is the stationary solution of the proportion of degree k dual vertices that has s splits. The results for N^* and N^{ES} under the DBMF approximation both with no degree correlation and with the general degree correlation are computed. Two metrics, namely, the mean absolute error

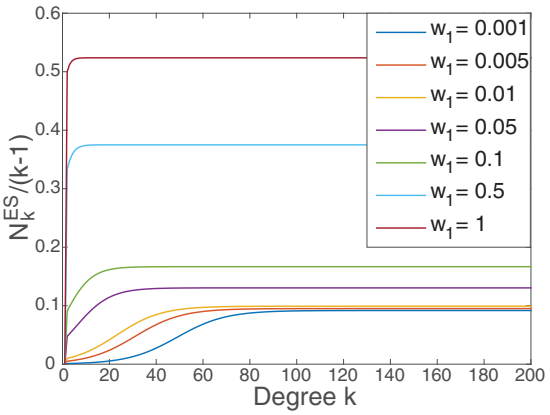

FIG. 10. Impact of w_1 on the expected level of functional loss $[N_k^{ES}/(k-1)]$ for dual vertices of different degrees ($w_2 = 0.1$, $w_3 = 0$).

(MAE) and mean relative error (MRE), are used for evaluation; they are computed as

$$\mathcal{E}_{\mathrm{MAE}} = \frac{\sum_{i=1}^{n} |d_i - \hat{d}_i|}{n}, \quad \mathcal{E}_{\mathrm{MRE}} = \frac{\sum_{i=1}^{n} |d_i - \hat{d}_i|}{\sum_{i=1}^{n} d_i},$$

where d_i is the empirical observation i and $\hat{d}_i$ is the value computed using the vertex split-recovery model. Figures 8 and 9 present the sample results for a typical weekday and a weekend for both the Beijing and the Shanghai road networks (for complete results see the Supplemental Material [43]).

The comparison results show that N^* and N^{ES} computed from the vertex split-recovery model generally agree with the patterns of empirical data. It is found that for the total number of dual vertices N^*, the MRE and MAE for the Beijing road network are less than 2.5% and 150, respectively. For the Shanghai road network, the MRE and MAE are less than 1.5% and 80, respectively. For the total expected number of vertex splits N^{ES}, the MRE and MAE for the Beijing road network are less than 16% and 105, respectively. The MRE and MAE results for the Shanghai road network are less than 11% and 72, respectively. On weekends, when the traffic loading level is lower, even smaller MAE and MRE results are achieved for both cities.

It should be noted that N^* and N^{ES} are obtained using the stationary solution of the vertex split-recovery model, which corresponds to a stable network configuration under a constant traffic loading level after a sufficiently long observation period. As real-world traffic loading is constantly changing, such a stable network configuration is not easily achievable. It is reasonable to expect a certain level of discrepancy between the empirical data and the predictions of the model. Considering the relatively low MAE and MRE values, the vertex split-recovery model provides a reasonably good approximation of the real-world congestion evolution process.

B. Expected functional loss for dual vertices

There is a minor difference in the dual-vertex degree distribution results between the DBMF approximation with no degree and that with the general degree correlation (Fig. 6). This is because considering the general degree correlation only improves the approximation of the neighbor-contagion process. Given that the normalized neighbor-contagion rate w_3 is very low compared with other parameters, the impact of considering the degree correlation is limited.

As w_3 is very small, if we set $w_3 = 0$, we can approximate the expected number of vertex splits for dual vertices of degree k ($k > 1$) under the stationary solution in closed form:

$$N_k^{ES} = \sum_{s=1}^{k-1} s \cdot x_s^{k*} \approx \frac{w_1(k-1)(1+w_1+w_2)^{k-2}}{1 + \frac{w_1}{w_1+w_2}[(1+w_1+w_2)^{k-1} - 1]}. \tag{21}$$

When normalized by the maximum possible number of vertex splits $k-1$, it can be shown that $\frac{N_k^{ES}}{k-1} \leqslant \frac{w_1+w_2}{1+w_1+w_2}$ and the equal sign is attainable only when $k \to \infty$. The quantity $N_k^{ES}/(k-1)$ can be perceived as a measure of the expected level of functional loss for dual vertices of degree k, for which $N_k^{ES}/(k-1) = 0$ indicates that that no congestion is present and a value of 1 indicates that all segments of the road are congested.

Figure 10 presents the impact of w_1 on $N_k^{ES}/(k-1)$ for dual vertices of different degrees. $N_k^{ES}/(k-1)$ converges to

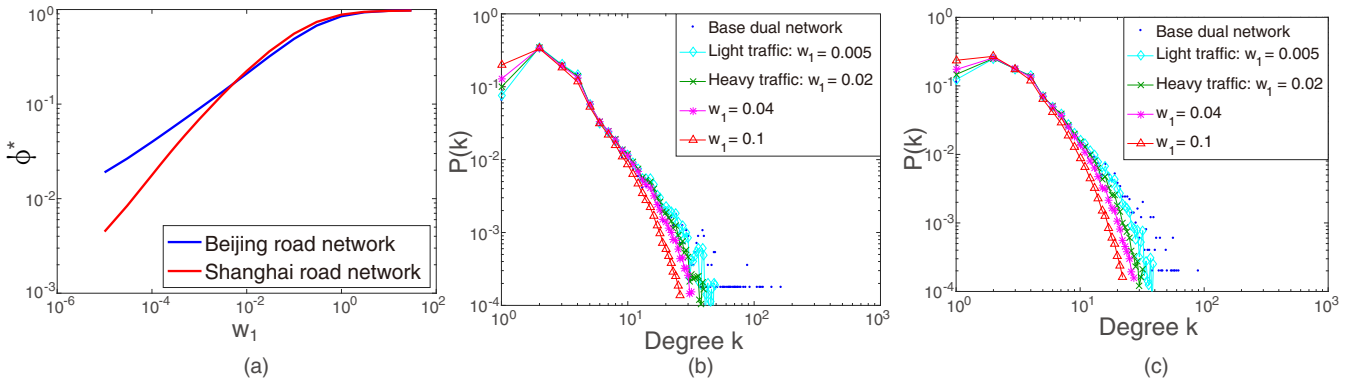

FIG. 11. Comparison of network performance under different normalized network loading levels. (a) Impact of w_1 on the average probability that a dual vertex has a split neighbor under the stationary solution (ϕ^*). Obtained by solving for the stationary solution under the DBMF approximation with no degree correlation assumption. (b), (c) Plots of the dual degree distributions of the Beijing and Shanghai road networks under the same set of normalized network loading levels. The light-traffic condition is taken as the typical w_1 value in late-night hours; the heavy-traffic condition is selected as the typical peak-hour w_1 value.

$\frac{w_1+w_2}{1+w_1+w_2}$ as k becomes large. This leads to an interesting observation: that although high-dual-degree vertices are more likely to experience vertex split, they seem to converge to the same level of expected functional loss. In the vertex split-recovery model, dual vertices with more splits have a higher recovery rate (more congested segments are likely to recover), which suppresses dual vertices from further splitting. This is similar to the existence of the equilibrium state between the susceptible and the infected population in the susceptible-infected-susceptible model. One possible real-world explanation is that, a severely congested road will lose a considerable fraction of functional connectivity, which might forbid further entry and propagation of traffic flow; this in turn could impede the further worsening of congestion. Another possible explanation is related to the moving jam effect [44,45], where the road segments get congested and then recover as the jam moves along the road. In this situation, although congestion is present, the road maintains a certain functional level.

C. Network performance

The vertex split-recovery model can serve as a simple but powerful tool in analyzing network performance under real or hypothetical traffic loads. Figure 11(a) plots the impact of w_1 on the average probability that a dual vertex has a split neighbor ϕ^*. A high value of ϕ^* corresponds to a heavily congested network. We find that the Shanghai network performs better than the Beijing road network under light traffic loading levels but tends to perform slightly worse under high loading situations. As mentioned previously, the Shanghai network is less hierarchical and gridlike, making it more resistive to the emergence of congestion but, at the same time, opening more channels for the further propagation of congestion, causing worse performance at high loading levels. On the contrary, the Beijing road network depends more on major ring and radial expressways, which increases the chances of the emergence of congestion. The existence of high-capacity major roads also allows for handling a higher traffic volume and the hierarchical structure reduces potential congestion propagation pathways under high traffic loading. The differences in the network performances is further reflected in the dual degree distributions of the function-augmented dual networks. Figures 11(b) and 11(c) present a comparison of the two networks under the same set of network loading levels. A larger extent of deviation of the dual degree distribution is observed in the Shanghai network under high network loading levels compared to the Beijing road network.

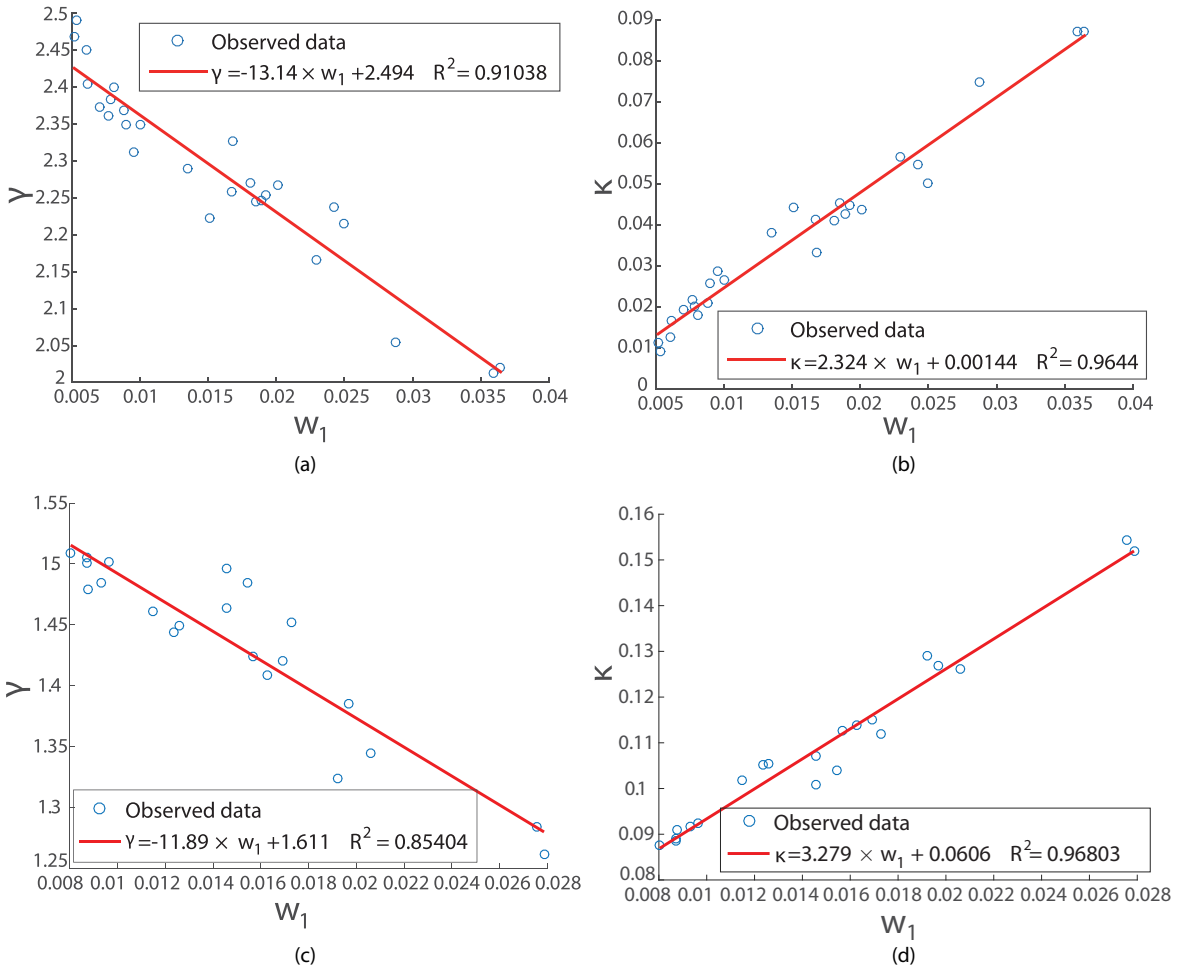

FIG. 12. Relationship of the parameters of the power law with an exponential cutoff distribution and the fitted w_1 value. (a), (b) Linear fitting of the γ-w_1 and κ-w_1 relationships for the Beijing road network (12/11/2015). (c), (d) Linear fitting of the γ-w_1 and κ-w_1 relationships for the Shanghai road network (7/11/2016).

Another interesting finding is the close relationship of the vertex split-recovery model with the emergence of exponential cutoff behavior in the dual degree distribution. As shown in Fig. 6, a power law with an exponential cutoff distribution [$P(k) \sim k^{-\gamma} e^{-\kappa k}$] can serve as an excellent approximation of the stationary solution of the vertex split-recovery model for $k \geqslant k_{\min}$ ($k_{\min} = 3$ for Beijing network and $k_{\min} = 4$ for Shanghai network). Unfortunately, the complex mathematical form of the stationary solution forbids the analytical derivation of this corresponding relationship. However, compared with the fitted normalized network load level w_1 and the parameters of γ and κ, a remarkably simple linear relationship can be shown. Figure 12 presents the sample results of the γ-w_1 and κ-w_1 relationships for the Beijing and Shanghai road networks. We observe that $\gamma \approx \alpha_0 - \alpha_1 w_1$ and $\kappa \approx \alpha_2 w_1$ (the constant term in the κ-w_1 linear fitting is relatively small and can be ignored), where α_0, α_1, and α_2 are positive constants. This analysis shows that the normalized network loading level w_1 plays a central role, causing the dual-vertex degree distribution of a function-augmented dual network to deviate from a power-law distribution and the emergence of exponential cutoff behavior.

VI. CONCLUSION

Our theoretical analysis, combined with observational data from two megacities in China, enables examination and prediction of how functional failures (traffic congestion) and recoveries evolve in structurally intact road networks. We have successfully described the deviation of the dual-vertex degree distribution from a power-law distribution and the emergence of exponential cutoff behavior under congestion using a vertex split-recovery model. The model links the network-level functional loss with the traffic loading level and provides a statistical characterization of the likelihood of experiencing functional failures for dual vertices. We also show that certain network topological features can amplify network functional failures through negative feedbacks, while other topological features can suppress congestion cascading. The evolution of functional failure depends on the interaction of network topology and loading. The gridlike road network in Shanghai performs better at low traffic loadings but propagates congestion at higher loadings. In contrast, the ring-and-radial structure of the Beijing road network allows higher traffic volumes but is vulnerable to the emergence of congestion.

Performing functional analysis by overlaying real-world flow propagation principles on the structural details of flow-based networks is a challenging problem due to the need to model flows. Our work provides a new scientific approach to tackling this complex problem. Instead of analyzing the flow pattern in the network, we can model the flow-induced functional process as an equivalent structural process. The vertex split-recovery model is a perfect example showing how traffic congestion in road networks can be modeled as a structural process in a transformed graph, which combines both the flow propagation principle of traffic and the network structure. By finding appropriate equivalent structural processes for different types of flow and networks, a similar analytical approach can be applied to other flow-based networks. Future research can further explore such equivalent structural processes and develop a generalized theory for flow-based complex networks.

ACKNOWLEDGMENTS

This work was partially funded by "NSF Collaborative Research RIPS Type 2: Resilient Simulation for Water, Power, and Road Networks" (lead-PI: P. Suresh C. Rao). The work of Satish Ukkusuri is partly funded by NSF Grant No. 1638311 CRISP Type 2/Collaborative Research: Critical Transitions in the Resilience and Recovery of Interdependent Social and Physical Networks.

APPENDIX A: CONSTRUCTION OF A FUNCTION-AUGMENTED DUAL NETWORK

The vertex split-recovery process is defined in function-augmented dual networks. We use two procedures to construct the function-augmented dual network at each time step. We first construct the base dual network using the hierarchical intersection continuity negotiation (HICN) dual-mapping technique [25]. HICN dual mapping merges consecutive road segments into the same dual vertex if they belong to the same road class and the convex angle they form is close to 180°. Details of the HICN dual-mapping procedure can be found in Algorithm I. Once the base dual road network is constructed, we overlay the functional states on the network and perform functional dual mapping to track the split-recovery trajectory for each dual vertex at each time step. Details of the functional dual-mapping procedure can be found in Algorithm II.

Algorithm 1: HICN dual-mapping procedure.

1. Scan the primal network, and put all primal edges into the unused edge set E_N. Let the used edge set $E_U = \emptyset$, dual vertex set $V_D = \emptyset$, and dual edge set $E_D = \emptyset$.
2. If $E_N \neq \emptyset$, pick a primal edge e_P from E_N and create a candidate edge $e_{CD} = e_P$; otherwise, go to step 4.
3. Grow e_{CD} by recursively executing the following until e_{CD} cannot be extended further:
   (a) Inspect the two end points of e_{CD}. For each end point, if it connects to any edge $e \in E_N$, compute the convex angle θ_i for e_{CD} and e_i.
   (b) Merge e_{CD} and e_i if the following conditions are satisfied:
      i. e_{CD} and e_i are of the same road class.
      ii. $\theta_i = \max\{\theta_1, \theta_2, \dots\}$ and $\theta_i < \theta_{\max}$, where $\theta_{\max}$ is the predefined maximum threshold angle ($\pi/3$ used in the actual implementation).
   (c) If e_{CD} and e_i can be merged, then $e_{CD} \leftarrow e_{CD} \bigcup \{e_i\}$, $E_N \leftarrow E_N \setminus e_i$, $E_U \leftarrow E_U \bigcup \{e_i\}$.
4. Create the dual vertex $v_D = e_{CD}$ and let $V_D \leftarrow V_D \bigcup \{v_D\}$. Go back to step 2.
5. Construct the dual-mapped network. For every two dual vertices v_{D_i} and v_{D_j} represented as a set of primal edges, if they contain primal edges that intersect each other, construct a dual edge $e_{D_{ij}}$ between v_{D_i} and v_{D_j}.

Algorithm 2: Functional dual-mapping procedure.

1. Create the base dual road network $G_D^0(V_D^0, E_D^0)$ using Algorithm I.
2. At time step t, for each dual vertex $v_{D_i}^{t-1} \in V_D^{t-1}$:
   (a) Let $V_D^t = \emptyset$, $E_D^t = \emptyset$.
   (b) Scan the functional state of each primal edge contained in $v_{D_i}^{t-1}$:
      i. If any primal road segments are in a failed state (congested), split the dual vertex $v_{D_i}^{t-1}$ into a set of new dual nodes $V_S = \{V_{D_{i1}}^t, \ldots, V_{D_{is}}^t\}$ at the locations of the failed road segments. Set $V_D^t \leftarrow V_D^t \bigcup V_S$.
      ii. Otherwise, set $v_{D_i}^t = v_{D_i}^{t-1}$. Set $V_D^t \leftarrow V_D^t \bigcup \{v_{D_i}^t\}$.
3. For all dual vertices $\tilde{V}_{D_i} = \{v_{D_{i1}}^t, v_{D_{i2}}^t, \ldots, V_{D_{is}}^t\}$ that originally evolved from $v_{D_i}^0$, check the primal edges in the working state (not congested) that are contained in $v_{D_i}^0$ but not in dual vertices in $\tilde{V}_{D_i}$. Merge the dual vertices at the location of such primal edges and update the dual vertices in $\tilde{V}_{D_i}$ as well as V_D^t accordingly.
4. Build the dual-mapped network $G_D^t(V_D^t, E_D^t)$. For each pair of dual nodes $v_{D_i}^t$ and $v_{D_j}^t$ in V_D^t, add a dual edge $e_{D_{ij}}$ to E_D^t if v_{D_i} and v_{D_j} share a common primal vertex.

APPENDIX B: DERIVATION OF THE RECURSIVE FORMULATION FOR THE MICROSCOPIC-LEVEL MODEL

For $S > 1$ and $i = 1,2,\ldots,k-S-1$, it can be proved that the following recursive formulation holds for the expected number of split subvertices of degree i for a dual vertex of degree k after S splits:

$$m_i(k,S+1) = \frac{k-S-i}{k-S-1} m_i(k,S) + \frac{1}{k-S-1} \sum_{s=i+1}^{k-S} (s-1) m_s(k,S) m_i(s,1). \tag{B1}$$

Proof. Consider a dual vertex of degree k after S splits (remove the effect of historical vertex recoveries). If we perform one more split (suppose that $S < k-1$), the probability of selecting a leaf vertex of degree s is

$$m_s(k,S) \cdot \frac{s-1}{k-S-1},$$

as the probability of selecting a leaf vertex of degree s is proportional to $s-1$. Splitting this vertex will decrease the expected number of leaf vertices of degree s by 1 but increase the expected number of leaf vertices of degree other than s by $M(s,1)$. Hence the expected change in M after splitting this vertex is

$$\Delta_s^M = m_s(k,S) \cdot \frac{s-1}{k-S-1} [M(s,1) - E_s],$$

in which E_s is a vector where only the sth element is 1, and all others are 0. The expected number of subvertices of different degrees for a dual vertex of degree k after $S+1$ splits can be obtained by summing Δ_s^M for all possible s values ($s = 1,2,\ldots,k-S$):

$$\begin{aligned} m_i(k,S+1) &= m_i(k,S) + \sum_{s=1}^{k-S} \Delta_s^M \\ &= \frac{k-S-i}{k-S-1} m_i(k,S) + \frac{1}{k-S-1} \sum_{s=i+1}^{k-S} (s-1) m_s(k,S) m_i(s,1). \end{aligned}$$

We hence obtained the recursive formulation for computing $m_i(k,S)$. Note that in the above derivation, we have used the fact that $m_i(s,1) = 0$ for $i \geqslant 0$. ■

APPENDIX C: CLOSED-FORM SOLUTION OF EQ. (3) UNDER $\beta = 0$

The closed-form expression of the recursive formulation, Eq. (3), is not known. However, the reduced uniform split case $\beta = 0$ can be analytically derived as follows:

$$m_i(k,S) = \begin{cases} \frac{S(S+1)}{k-S} \prod_{j=1}^{S-1} \left(1 - \frac{i}{k-j}\right), & i \leqslant k-S; \\ 0, & i > k-S. \end{cases} \tag{C1}$$

Proof. If $\beta = 0$, then we have uniform split, that is, $P(i,k-i|k) = 1/(k-1)$, and

$$m_i(k,1) = \begin{cases} \frac{2}{k-1}, & i < k; \\ 0, & i \geqslant k. \end{cases}$$

We prove the validity of the closed-form expression using induction. When $S = 1$, the expression obviously holds. Assume that the expression holds for $S \leqslant c$; then

$$\begin{aligned} m_i(k,c+1) &= \frac{k-c-i}{k-c-1} m_i(k,c) + \frac{1}{k-c-1} \sum_{s=i+1}^{k-c} (s-1) m_s(k,c) m_i(s,1) \\ &= \frac{k-c-i}{k-c-1} m_i(k,c) + \frac{2}{k-c-1} \sum_{s=i+1}^{k-c} m_s(k,c). \end{aligned}$$

As

$$\begin{aligned} m_s(k,c) &= \frac{c(c+1)}{k-c} \prod_{j=1}^{c-1} \left(1 - \frac{s}{k-j}\right) \\ &= \frac{c(c+1) \prod_{r=1}^{c-1} (k-r-s)}{\prod_{j=1}^{c} (k-j)}, \end{aligned}$$

$$\begin{aligned} \sum_{s=i+1}^{k-c} m_s(k,c) &= \frac{c(c+1)}{\prod_{j=1}^{c} (k-j)} \\ &\quad \times \sum_{s=i+1}^{k-c} \prod_{r=1}^{c-1} (k-r-s). \end{aligned}$$

Let

$$F_s = \prod_{r=1}^{c-1}(k-r-s), \quad G_s = s \cdot F_s.$$

Thus

$$F_{s+1} = \frac{k-(c-1)-(s+1)}{k-1-s}F_s = \frac{k-c-s}{k-s-1}F_s.$$

Then

$$kF_{s+1} - (s+1)F_{s+1} = (k-c)F_s - s \cdot F_s.$$

We have

$$kF_{s+1} - G_{s+1} = (k-c)F_s - G_s.$$

Summing the cases for $s = i+1$ to $k-c$,

$$k\sum_{s=i+1}^{k-c} F_{s+1} - \sum_{s=i+1}^{k-c} G_{s+1} = (k-c)\sum_{s=i+1}^{k-c} F_s - \sum_{s=i+1}^{k-c} G_s.$$

Note that $F_{k-c+1} = 0$, $G_{k-c+1} = 0$, thus

$$\sum_{s=i+1}^{k-c} F_{s+1} = \sum_{s=i+1}^{k-c} F_s - F_{i+1},$$

$$\sum_{s=i+1}^{k-c} G_{s+1} = \sum_{s=i+1}^{k-c} G_s - G_{i+1}.$$

Thus

$$c\sum_{s=i+1}^{k-c} F_s - kF_{i+1} + G_{i+1} = 0,$$

and

$$\sum_{s=i+1}^{k-c} F_s = \frac{k-i-1}{c}F_{i+1}.$$

Consequently,

$$\begin{aligned} m_i(k,c+1) &= \frac{k-c-i}{k-c-1}m_i(k,c) + \frac{2c(c+1)}{\prod_{j=1}^{c+1}(k-j)} \\ &\quad \cdot \frac{k-i-1}{c}\prod_{r=1}^{c-1}(k-r-i-1) \\ &= \frac{c(c+1)\prod_{r=1}^{c}(k-r-i)}{\prod_{j=1}^{c+1}(k-j)} \\ &\quad + \frac{2(c+1)\prod_{r=1}^{c}(k-r-i)}{\prod_{j=1}^{c+1}(k-j)} \\ &= \frac{(c+1)(c+2)}{k-c-1}\prod_{j=1}^{c}\left(1-\frac{i}{k-j}\right). \end{aligned}$$

We have proved that the proposed expression also holds for $m_i(k,c+1)$; by induction, the claim holds. ■

[1] R. Albert, I. Albert, and G. L. Nakarado, Phys. Rev. E **69**, 025103(R) (2004).

[2] D. J. Ashton, T. C. Jarrett, and N. F. Johnson, Phys. Rev. Lett. **94**, 058701 (2005).

[3] B. Danila, Y. Sun, and K. E. Bassler, Phys. Rev. E **80**, 066116 (2009).

[4] M. Barthélemy, Phys. Rep. **499**, 1 (2011).

[5] C. D. Brummitt, R. M. D'Souza, and E. A. Leicht, Proc. Natl. Acad. Sci. USA **109**, E680 (2012).

[6] D. Li, B. Fu, Y. Wang, G. Lu, Y. Berezin, H. E. Stanley, and S. Havlin, Proc. Natl. Acad. Sci. USA **112**, 669 (2015).

[7] J. Zhao, D. Li, H. Sanhedrai, R. Cohen, and S. Havlin, Nat. Commun. **7**, 10094 (2016).

[8] T. J. Brodribb, D. Bienaimé, and P. Marmottant, Proc. Natl. Acad. Sci. USA **113**, 4865 (2016).

[9] M. Garavello and B. Piccoli, *Traffic Flow on Networks* (American Ianstitute of Mathematical Sciences, Springfield, MO, 2006), Vol. 1.

[10] M. Patriksson, *The Traffic Assignment Problem: Models and Methods* (Courier Dover, Mineola, NY, 2015).

[11] S. Scellato, L. Fortuna, M. Frasca, J. Gómez-Gardeñes, and V. Latora, Eur. Phys. J. B **73**, 303 (2010).

[12] A. Solé-Ribalta, S. Gómez, and A. Arenas, R. Soc. Open Sci. **3**, 160098 (2016).

[13] D. S. Johnson, J. K. Lenstra, and A. Kan, Networks **8**, 279 (1978).

[14] R. Guimerà, A. Díaz-Guilera, F. Vega-Redondo, A. Cabrales, and A. Arenas, Phys. Rev. Lett. **89**, 248701 (2002).

[15] A. Tomaszewski, M. Pióro, and M. Żotkiewicz, Networks **55**, 108 (2010).

[16] R. Guimerà, A. Arenas, A. Díaz-Guilera, and F. Giralt, Phys. Rev. E **66**, 026704 (2002).

[17] J. Duch and A. Arenas, Phys. Rev. Lett. **96**, 218702 (2006).

[18] D. De Martino, L. Dall'Asta, G. Bianconi, and M. Marsili, Phys. Rev. E **79**, 015101 (2009).

[19] L. A. Briggs and M. Krishnamoorthy, Proc. Natl. Acad. Sci. USA **110**, 19295 (2013).

[20] A. Rinaldo, R. Rigon, J. R. Banavar, A. Maritan, and I. Rodriguez-Iturbe, Proc. Natl. Acad. Sci. USA **111**, 2417 (2014).

[21] A. Solé-Ribalta, S. Gómez, and A. Arenas, Phys. Rev. Lett. **116**, 108701 (2016).

[22] T. C. Jarrett, D. J. Ashton, M. Fricker, and N. F. Johnson, Phys. Rev. E **74**, 026116 (2006).

[23] S. Porta, P. Crucitti, and V. Latora, Physica A **369**, 853 (2006).

[24] B. Jiang, Physica A **384**, 647 (2007).

[25] A. P. Masucci, K. Stanilov, and M. Batty, Phys. Rev. E **89**, 012805 (2014).

[26] E. Krueger, C. Klinkhamer, C. Urich, X. Zhan, and P. S. C. Rao, Phys. Rev. E **95**, 032312 (2017).

[27] M. J. Lighthill and G. B. Whitham, Proc. R. Soc. Lond. A **229**, 317 (1955).

[28] C. F. Daganzo, Transport. Sci. **32**, 3 (1998).
[29] B. S. Kerner, Phys. Rev. E **84**, 045102 (2011).
[30] D. R. Cox and D. Oakes, *Analysis of Survival Data* (CRC Press, Boca Raton, FL, 1984), Vol. 21.
[31] J. F. Lawless, *Statistical Models and Methods for Lifetime Data* (John Wiley & Sons, New York, 2011), Vol. 362.
[32] R. Sainudiin and A. Véber, Roy. Soc. Open Sci., **3**, 5 (2016).
[33] D. Aldous, in *Random Discrete Structures* (Springer, Berlin, 1996), pp. 1–18.
[34] B. Chen, D. Ford, and M. Winkel, Electron. J. Prob. **14**, 400 (2009).
[35] M. G. B. Blum and O. François, Syst. Biol. **55**, 685 (2006).
[36] R. M. Anderson and R. M. May, *Infectious Diseases of Humans: Dynamics and Control* (Oxford University Press, Oxford, 1992).
[37] R. Pastor-Satorras and A. Vespignani, Phys. Rev. Lett. **86**, 3200 (2001).
[38] A. Barrat, M. Barthelemy, and A. Vespignani, *Dynamical Processes on Complex Networks* (Cambridge University Press, Cambridge, 2008).
[39] S. N. Dorogovtsev, A. V. Goltsev, and J. F. F. Mendes, Rev. Mod. Phys. **80**, 1275 (2008).
[40] R. Pastor-Satorras, C. Castellano, P. Van Mieghem, and A. Vespignani, Rev. Mod. Phys. **87**, 925 (2015).
[41] M. Newman, *Networks: An Introduction* (Oxford University Press, New York, 2010).
[42] J. Lin, IEEE Trans. Info. Theory **37**, 145 (1991).
[43] See Supplemental Material at http://link.aps.org/supplemental/10.1103/PhysRevE.96.052301 for additional information and results.
[44] B. S. Kerner, J. Phys. A **33**, L221 (2000).
[45] B. S. Kerner, S. L. Klenov, A. Hiller, and H. Rehborn, Phys. Rev. E **73**, 046107 (2006).